Inorg. Chem. **2008**, *47*, 10911−10920

Molecular and Electronic Structure of the Square Planar Bis(*o*-amidobenzenethiolato)iron(III) Anion and Its Bis(*o*-quinoxalinedithiolato)iron(III) Analogue

Nabarun Roy, Stephen Sproules, Eckhard Bill, Thomas Weyhermüller, and Karl Wieghardt*

Max-Planck-Institut für Bioanorganische Chemie, Stiftstrasse 34-36, D-45470 Mülheim an der Ruhr, Germany

Received June 16, 2008

Crystalline purple $[PPh_4][Fe^{III}L_2]$ (**1**), where L^{2-} represents the closed-shell dianion of 4,6-di-*tert*-butyl-2-[(pentafluorophenyl)amino]benzenethiol, has been synthesized from the reaction of H_2L and $FeBr_2$ (2:1) in acetonitrile with excess NEt_3, careful, brief exposure of the solution to air, and addition of $[PPh_4]Br$. The monoanion has been shown by X-ray crystallography to be square planar. The oxidation of **1** with 1 equiv of iodine produces the neutral species $[FeI(L^{\bullet})_2]^0$ (**2**) where $(L^{\bullet})^{1-}$ represents the one-electron oxidized π radical anion of L^{2-}. The reaction of H_2L and $PtCl_2$ (2:1) and NEt_3 in CH_3CN in the presence of air produced green, crystalline $[Pt^{II}(L^{\bullet})_2]$ (**3**). From temperature-dependent (2−300 K) magnetic susceptibility measurements, it was established that **1** possesses a central intermediate spin ferric ion ($S_{Fe} = {}^3/_2$), whereas neutral **2** has a doublet ground state ($S_t = {}^1/_2$) comprising an intermediate spin ferric ion coupled antiferromagnetically to two ligand π radicals $(L^{\bullet})^{1-}$ ($S_{rad} = {}^1/_2$). Complex **3** is diamagnetic. Almeida et al.'s complexes in ref 1, $[N(n\text{-}Bu)_4][Fe^{III}(qdt)_2]$ (**A**), and $[PPh_4]_2[Fe^{III}_2(qdt)_4]$ (**B**), have been revisited. It is shown here that the square planar anion in mononuclear $[Fe^{III}(qdt)_2]^-$ also possesses an $S_{Fe} = {}^3/_2$ ground state. The zero-field Mössbauer spectra of **1**, **2**, **A**, and **B** have been recorded and the molecular and electronic structures of all mononuclear iron species have been calculated by density functional theoretical methods. It is shown that the $S = {}^3/_2$ ground state in **1** and **A** is lower in energy by 8.5 and 16.6 kcal mol^{-1}, respectively, than the $S = {}^1/_2$ state.

Introduction

Monomeric, strictly four-coordinate square planar complexes of iron(III) (d^5) are relatively rare.[1−4] Only recently in 2008 has such a four-coordinate (porphyrinato)Fe(III) cation been structurally characterized by Suslick et al.[3] A similar octamethylporphyrinogen complex of iron(III) containing a tetradentate tetraanionic ligand L^{4-} has been carefully investigated by Bachmann and Nocera in 2004.[2] The electronic structure of all of these complexes has been described as comprising an intermediate spin ferric ion (d^5, $S_{Fe} = {}^3/_2$) in full agreement with simple qualitative ligand field theoretical expectations.

Scheme 1. Complexes from Ref 1

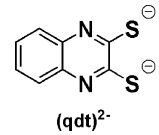

$(qdt)^{2-}$

$[N(n\text{-}Bu)_4][Fe^{III}(qdt)_2]$ **A**

$[AsPh_4]_2[Fe_2^{III}(qdt)_4]$

A square planar organo-iron(III) compound with a spin-admixed state has also been reported: $[Li(thf)_4][Fe^{III}(C_6Cl_5)_4]$ where $C_6Cl_5^-$ is the pentachlorophenyl anion.[4] This species possesses a spin-admixed ($S = {}^3/_2, {}^5/_2$) state as was deduced from EPR, Mössbauer spectroscopy, and temperature-dependent magnetic susceptibility measurements.

It is therefore rather surprising that the square planar monoanion bis(*o*-quinoxalinedithiolato)iron(III) shown in Scheme 1 has been reported to possess an $S = {}^1/_2$ ground state.[1] $[(n\text{-}Bu)_4N][Fe^{III}(qdt)_2]$ (**A**) has been structurally

* To whom correspondence should be addressed. E-mail: wieghardt@mpi-muelheim.mpg.de.

(1) Simão, D.; Ayllón, J. A.; Rabaça, S.; Figueira, M. J.; Santos, I. C.; Henriques, R. T.; Almeida, M. *Cryst. Eng. Comm.* **2006**, *8*, 658.
(2) Bachmann, J.; Nocera, D. G. *J. Am. Chem. Soc.* **2005**, *127*, 4730.
(3) Fang, M.; Wilson, S. R.; Suslick, K. S. *J. Am. Chem. Soc.* **2008**, *130*, 1134.
(4) Alonso, P. J.; Arauzo, A. B.; Forniés, J.; Garcia-Monforte, M. A.; Martin, A.; Martinez, J. I.; Menjón, B.; Rillo, C.; Sáiz-Garitaonandia, J. J. *Angew. Chem., Int. Ed.* **2006**, *45*, 6707.

10.1021/ic801109n CCC: $40.75
Published on Web 11/07/2008

Scheme 2. Ligands and Complexes of This Work

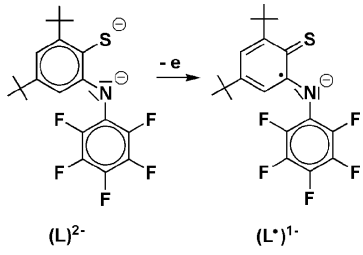

$[PPh_4][Fe^{III}L_2]$	(1)	(S = 3/2)
$[Fe^{III}I(L^{\bullet})_2]^0$	(2)	(S = 1/2)
$[Pt^{II}(L^{\bullet})_2]^0$	(3)	(S = 0)

characterized by X-ray crystallography; it contains a square planar FeS_4 moiety.[1] From temperature-dependent magnetic susceptibility measurements (4−300 K) an effective magnetic moment of 2.34 μ_B per iron ion, which is "almost temperature constant" between 297 and 25 K has been derived. A considerably large g value of 2.7 was deduced from this data. Interestingly, changing the $[N(n\text{-}Bu)_4]^+$ cation in **A** to $[AsPh_4]^+$ in $[AsPh_4]_2[Fe_2(qdt)_4]$ produces a dimer (Scheme 1) with two five-coordinate $Fe^{III}S_5$ polyhedra, as determined by X-ray crystallography.[1]

The reported electronic structure of the monomeric species **A** is very interesting because in simple ligand field theoretical terms a d^5 electron configuration should not lead to an $S = {}^1/_2$ ground state in a square planar ligand field. The asserted $S = {}^1/_2$ state can, in principle, be generated by an intermediate spin ferrous ion ($S_{Fe} = 1$) coupled antiferromagnetically to a ligand π radical $(qdt^{\bullet})^{1-}$ yielding $[Fe^{II}(qdt)(qdt^{\bullet})]^-$ ($S = {}^1/_2$). This would imply the presence of a redox noninnocent character of the ligand $(qdt)^{2-}$.

To fully characterize the electronic structure of such square planar ferric complexes containing thiolate ligands in more detail, we have synthesized and fully characterized the *first* square planar anion $[Fe^{III}L_2]^{1-}$ containing two *o*-aminothiophenolate(2−) ligands (trans-$Fe^{III}N_2S_2$) (Scheme 2). To clearly discern the closed-shell dianion $(L)^{2-}$ from its π radical monoanion $(L^{\bullet})^{1-}$, we have also prepared the complexes $[Fe^{III}I(L^{\bullet})_2]^0$ (**2**) and $[Pt^{II}(L^{\bullet})_2]^0$ (**3**) and established the structure of the latter by X-ray crystallography. Broken symmetry (BS) density functional theoretical (DFT) calculations[5,10] on **1**, **2**, **3**, and **A** have also been performed, which clearly support the notion that the square planar monoanions in **1** and **A** possess an $S = {}^3/_2$ ground state.

Experimental Section

The complex $[N(n\text{-}Bu)_4][Fe(qdt)_2]$ (**A**) has been prepared according to published procedure, while its dinuclear analogue $[PPh_4]_2[Fe_2(qdt)_4]$ (**B**) was adapted from the procedure for $[AsPh_4]_2[Fe_2(qdt)_4]$ published in ref 1. Slight variations are indicated in the Results section. The abbreviation $(qdt)^{2-}$ represents the ligand *o*-quinoxalinedithiolate(2−).

Synthesis of the ligand, H_2(L). (a) Preparation of 3,5-Di-*tert*-butylaniline. A solution of 3,5-di-*tert*-butylbenzoic acid (5.00 g; 21.3 mmol) in concentrated H_2SO_4 (15 mL) and $CHCl_3$ (15 mL) was heated to 45 °C, and NaN_3 (1.50 g; 23.1 mmol) was added over a period of an hour. Stirring was continued for five hours before $CHCl_3$ was removed under reduced pressure. The residue was cooled (0 °C) and ice water (150 mL) was added. The resulting precipitate was filtered and washed with water (100 mL). The precipitate, 3,5-di-*tert*-butylaniline sulfonate, was dissolved in methanol (25 mL), and an aqueous solution of KOH (5 g in 100 mL water) was added. The precipitate was filtered and washed with a large amount of water. The product was dried in air. Yield: 4.14 g (92%).

(b) Synthesis of *N*-(Pentafluorophenyl)-3,5-di-*tert*-butylaniline. A solution of dry 3,5-di-*tert*-butylaniline (4.00 g; 19.5 mmol) was prepared in dry THF (15 mL) and cooled to −78 °C. A solution of lithium bis-(trimethylsilyl)amide (6.53 g; 39.0 mmol) in THF (20 mL) was added dropwise under argon. The solution was stirred vigorously for 10 min, followed by the addition of hexafluorobenzene (3.63 g; 19.5 mmol). The reaction mixture was allowed to warm up to room temperature, and stirring was continued for three days. Water (100 mL) was added to the reaction mixture, and the product was extracted with diethyl ether (150 mL). The organic layer was dried over Na_2SO_4, and the solvent was removed in vacuo. The product was isolated as a yellow-orange oil. Yield: 5.21 g (72%). EI-MS: $m/z = 371$ $[M^+]$. ^1H NMR (500 MHz ($CDCl_3$)): δ 1.27 (s, 9H), 1.30 (s, 9H), 7.05−7.24 (m, 3H), 5.43 (s, 1H). Anal. Calcd for $C_{20}H_{22}NF_5$: C, 64.68; H, 5.97, N, 3.77. Found: C, 64.76; H, 6.13; N, 3.91.

(c) Preparation of 4,6-Di-*tert*-butyl-2-[(pentafluorophenyl)-amino]benzenethiol, H_2L. Freshly distilled S_2Cl_2 (1.30 mL, 16.3 mmol) was added dropwise over the course of 10 min to a solution of *N*-(pentafluoropheny)-3,5-di-*tert*-butylaniline (5.93 g; 16.0 mmol) in benzene (20 mL) warmed to 45−50 °C, and the solution was stirred for an hour. The reaction mixture was then heated to 75−80 °C, and granulated Zn (16 g) and concentrated hydrochloric acid (16 mL) were added very slowly in portions with vigorous stirring. Heating was continued for four hours under argon. The reaction mixture was then filtered, and the filtrate was washed with a large volume of water until the washings were pH neutral. Then the product was extracted into benzene (50 mL), and the extractants were dried over Na_2SO_4, before the solvent was removed under reduced pressure. The product was isolated as a yellow powder and stored under argon. Yield: 4.09 g (76%). IR (KBr disk): ν(N−H) 3349, ν(C−H) 2962, 2905, 2870 cm^{-1}. EI-MS: $m/z = 403$ $[M^+]$. ^1H NMR (500 MHz, $CDCl_3$): δ 1.24 (s, 9H), 1.47 (s, 9H), 7.06−7.34 (m, 2H), 6.1 (s, 1H), 3.2 (s, 1H). Anal. Calcd for $C_{20}H_{22}NSF_5$: C, 59.54; H, 5.5; N, 3.47; S, 7.94. Found: C, 59.56; H, 5.53; N, 3.72; S, 8.03.

Syntheses of Complexes. $[PPh_4][FeL_2]$ (1). Under anaerobic conditions (Ar atmosphere), the ligand H_2L (0.40 g; 0.99 mmol) was dissolved in dry acetonitrile (15 mL). To the yellow solution was added $FeBr_2$ (0.11 g; 0.51 mmol) and triethylamine (0.28 mL; 2.01 mmol) with stirring for 15 min at 20 °C under argon. The reaction vessel was opened to atmosphere, whereupon the brown solution turned dark purple. The solvent was removed in vacuo and replaced with CH_2Cl_2 (20 mL). $[PPh_4]Br$ (0.21 g; 0.50 mmol) was then added under argon in a glovebox with stirring for 15 min at 20 °C, followed by filtration through celite. The reaction volume was reduced to 5 mL by vacuum evaporation, and *n*-hexane was added (25 mL), whereupon a purple microcrystalline precipitate of $[PPh_4][FeL_2]$ (**1**) formed, which was separated by filtration and stored under an argon atmosphere. Single crystals of $[PPh_4][FeL_2]\cdot(C_2H_5)_2O$ (**1**) suitable for X-ray diffraction were grown by slow diffusion of diethylether into a CH_2Cl_2 solution of the crude purple product. Yield: 0.43 g (72%). Anal. Calcd for

(5) Chlopek, K.; Muresan, N.; Neese, F.; Wieghardt, K. *Chem.—Eur. J.* **2007**, *13*, 8390.

$C_{64}H_{60}F_{10}S_2N_2PFe$: C, 64.16; H, 5.04; N, 2.34; Fe, 4.66. Found: C, 64.20; H, 5.07; N, 2.38; Fe, 4.71. ESI-MS (positive ion, CH_2Cl_2): $m/z = 339.2$ $[PPh_4]^+$; negative ion $m/z = 858.2$ $[FeL_2]^-$.

[FeI(L$^{\bullet}$)$_2$] (2). Complex **1** (0.19 g; 0.16 mmol) was dissolved in dry dichloromethane (15 mL) under anaerobic conditions. To this dark violet solution was added I_2 (0.08 g; 0.32 mmol), dissolved in *n*-hexane (15 mL), whereupon a color change from dark violet to dark blue was observed. The reaction mixture was stirred under Ar for 20 min, and the solvent was removed under vacuum. The residue was redissolved in diethylether (20 mL) and filtered through celite. Evaporation of the solvent under reduced pressure yielded the product as a dark blue black microcrystalline solid. Yield: 0.08 g (51%). ESI-MS: $m/z = 985.1$ $\{M\}^+$. Anal. Calcd for $C_{40}H_{40}F_{10}S_2N_2FeI$: C, 48.74; H, 4.09; N, 2.84; Fe, 5.66; I, 12.87. Found: C, 48.25; H, 3.86; N, 2.88; Fe, 5.24; I, 13.26.

[Pt(L$^{\bullet}$)$_2$] (3). To a solution of the ligand H_2L (0.28 g; 0.69 mmol) in dry CH_3CN (15 mL) was added $PtCl_2$ (0.09 g; 0.34 mmol) and NEt_3 (0.20 mL; 1.43 mmol). The solution was stirred for 10 min under argon and was then exposed to air for ~5 min, whereupon the color of the solution changed from dark brown to dark green. The solvent was removed under pressure and the solids reconstituted in CH_2Cl_2 (15 mL). Slow evaporation from this solution afforded **3** as a green microcrystalline solid. Yield: 0.26 g (75%). Single crystals of **3** were grown by slow evaporation from a 2:1 CH_2Cl_2/CH_3CN solution of the complex. Anal. Calcd for $C_{40}H_{40}F_{10}S_2N_2Pt$: C, 48.14; H, 4.04; N, 2.81; Pt, 19.54. Found: C, 48.22; H, 4.16; N, 2.91; Pt, 19.62. ESI-MS (neg. ion; CH_2Cl_2): $m/z = 997.2$ $[PtL_2]^-$. The cyclic voltammogram of **3** in CH_2Cl_2 (0.10 M $[N(n\text{-}Bu)_4]PF_6$; 20 °C, glassy carbon working electrode, scan rate 100 mV s^{-1}) shows three reversible one-electron transfer waves at $E_{1/2} = 0.74$, −0.53, and −1.34 V versus the ferrocenium/ferrocene (Fc^+/Fc) couple which correspond to the couples $[\mathbf{3}]^+/[\mathbf{3}]^0$, $[\mathbf{3}]^0/[\mathbf{3}]^{1-}$, and $[\mathbf{3}]^{1-}/[\mathbf{3}]^{2-}$, respectively (see Supporting Information).

X-Ray Crystallographic Data Collection and Refinement of the Structures. A black single crystal of **1** and a dark green crystal of **3** were coated with perfluoropolyether, picked up with nylon loops, and were mounted in the nitrogen cold stream of a Bruker-Nonius KappaCCD diffractometer equipped with a Mo-target rotating-anode X-ray source. Graphite monochromated Mo Kα radiation ($\lambda = 0.71073$ Å) was used throughout. Final cell constants were obtained from least-squares fits of all measured reflections. Intensity data were corrected for absorption using intensities of redundant reflections. The structures were readily solved by Patterson methods and subsequent difference Fourier techniques. The Siemens ShelXTL[6] software package was used for solution and artwork of the structures; ShelXL97[7] was used for the refinement. All non-hydrogen atoms were anisotropically refined and hydrogen atoms were placed at calculated positions and refined as riding atoms with isotropic displacement parameters. Crystallographic data of the compounds are listed in Table 1.

The diethylether solvate molecule (O100−C104) and a phenyl ring (C81−C86) in the tetraphenylphosphonium cation in compound **1** were found to be disordered. Two split positions with an occupation ratio of about 53:47 were refined using a total of 31 restraints. Equal anisotropic displacement parameters were refined for corresponding split atoms employing the EADP instruction of ShelXL.[7] SAME and SADI instructions were utilized to restrain geometrical parameters of the split parts to be equal within errors.

Table 1. Crystallographic Data for **1** and **3**

	1	**3**
chemical formula	$C_{68}H_{70}F_{10}FeN_2OPS_2$	$C_{40}H_{40}F_{10}N_2PtS_2$
fw	1272.20	997.95
space group	$P\bar{1}$, No. 2	$P2_1/c$, No. 14
a, Å	13.3294(4)	5.9917(2)
b, Å	14.5221(4)	16.5057(5)
c, Å	17.4224(5)	21.1653(7)
α, deg	101.401(3)	90
β, deg	101.972(3)	101.414(3)
γ, deg	98.963(3)	90
V, Å	3165.2(2)	2051.79(11)
Z	2	2
T, K	100(2)	190(2)
ρ_{calcd}, g cm^{-3}	1.335	1.615
reflns collected/$2\Theta_{max}$	76 749/62.00	29 937/65.00
unique reflns/$I > 2\sigma(I)$	20 162/17 735	7399/4906
params/restraints	815/31	256/0
λ, Å /μ(Kα), cm^{-1}	0.71073/4.03	0.71073/35.97
R1 [a]/GOF [b]	0.0530/1.016	0.0352/1.005
wR2 [c] ($I > 2\sigma(I)$)	0.1130	0.0601
residual density, eÅ^{-3}	+1.19/−1.15	+0.71/−0.93

[a] Observation criterion: $I > 2\sigma(I)$. $R1 = \Sigma||F_o| - |F_c||/\Sigma|F_o|$. [b] $GOF = [\Sigma[w(F_o^2 - F_c^2)^2]/(n - p)]^{1/2}$. [c] $wR2 = [\Sigma[w(F_o^2 - F_c^2)^2]/\Sigma[w(F_o^2)^2]]^{1/2}$, where $w = 1/\sigma^2(F_o^2) + (aP)^2 + bP$, $P = (F_o^2 + 2F_c^2)/3$.

Physical Measurements. The equipment used for IR, UV−vis, EPR, and Mössbauer spectroscopies has been described in refs 8 and 9. The temperature-dependent magnetic susceptibilities of solid samples of complexes were measured by using a SQUID magnetometer (Quantum Design) at 1.0 T magnetic field in the range of 2−300 K. Corrections for underlying diamagnetism were made by using tabulated Pascal's constants. Spin Hamiltonian simulations of EPR spectra were performed with the XSOPHE program written by Hanson et al., which is distributed by Bruker Biospin GmbH. Ligand hyperfine interactions, including quadrupole interactions, were considered with the full-matrix approach. Cyclic voltammetry and coulometric experiments were performed using an EG&G potentiostat/galvanostat. All potentials are referenced versus the ferrocenium/ferrocene (Fc^+/Fc) couple.

Calculations. All DFT calculations were performed with the ORCA program package.[10] The geometry optimizations of iron complexes were carried out at the B3LYP level[11,12] of DFT. Scalar relativistic correction for iodine and Pt in **2** and **3**, respectively, were included using the zeroth-order regular approximation (ZORA) method.[13] All other details are described in ref 5 including the use of corresponding,[14] canonical, and quasi-restricted[15] orbitals; density plots were generated with Molekel.[16] Nonrelativistic, single-point calculations on the optimized geometries of iron complexes with the B3LYP functional were carried out to predict Mössbauer spectral parameters (isomer shift and quadrupole splittings). The calculations employed the CP(PPP) basis set[17] for iron and the

(6) *ShelXTL 6.14*; Bruker AXS Inc.: Madison, WI, 2003.
(7) Sheldrick, G. M. *ShelXL97*; University of Göttingen: Göttingen, Germany, 1997.
(8) (a) Ghosh, P.; Bill, E.; Weyhermüller, T.; Wieghardt, K. *J. Am. Chem. Soc.* **2003**, *125*, 3967. (b) Ghosh, P.; Begum, A.; Bill, E.; Weyhermüller, T.; Wieghardt, K. *Inorg. Chem.* **2003**, *42*, 3208.
(9) Ray, K.; Bill, E.; Weyhermüller, T.; Wieghardt, K. *J. Am. Chem. Soc.* **2005**, *127*, 5641.
(10) Neese, F. *ORCA—An Ab Initio, Density Functional Theoretical and Semiempirical Electronic Structure Package*, version 2.6, revision 4; Institut für Physikalische und Theoretische Chemie, Universität Bonn: Bonn, Germany, 2007.
(11) Becke, A. D. *J. Chem. Phys.* **1986**, *84*, 4524.
(12) (a) Becke, A. D. J. *Chem. Phys.* **1993**, *98*, 5648. (b) Lee, C. T.; Yang, W. T.; Parr, R. G. *Phys. Rev.* **1988**, *37*, 785.
(13) (a) van Wüllen, C. *J. Chem. Phys.* **1998**, *109*, 392. (b) van Lenthe, E.; Baerendo, E. J.; Snijders, J. G. *J. Chem. Phys.* **1993**, *99*, 4597.
(14) Neese, F. *J. Phys. Chem. Solids* **2004**, *65*, 781.
(15) Schöneboom, J. C.; Neese, F.; Thiel, W. *J. Am. Chem. Soc.* **2005**, *127*, 5840.
(16) Molekel, advanced interactive 3D-graphics for molecular sciences, available at http://www.cscs.ch/molekel/.
(17) Neese, F. *Inorg. Chim. Acta* **2002**, *337*, 181.

Scheme 3. Synthesis of the Ligand H_2L

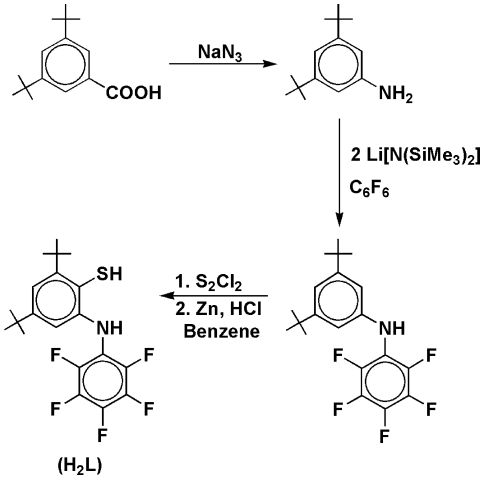

TZV(P) basis sets for N, S, and C atoms.[18] The SV(P) basis sets were used for the remaining atoms. The Mössbauer isomer shifts were calculated from the computed electron densities at the iron centers as described previously.[19] For some of the complexes studied in this work, we used the broken symmetry (BS) approach.[20] We adopted the following notation: the given system was divided into two fragments. The notation BS(m,n) refers then to a broken symmetry state with m unpaired spin-up electrons essentially on fragment 1 and n unpaired spin-down electrons localized on fragment 2. In most cases, fragments 1 and 2 correspond to the metal and the ligands, respectively. In this notation the standard high spin, open-shell solution is written as BS($m + n$,0). The BS(m,n) notation refers to the initial guess to the wave function. The variational process does, however, have the freedom to converge to a solution of the form BS($m - n$,0), in which effectively the n-spin-down electrons pair up with $n < m$ spin-up electrons on the partner fragment. Such a solution is then a standard $M_S \cong (m - n)/2$ spin-unrestricted Kohn−Sham solution.

As explained elsewhere,[14] the nature of the solution is investigated from the corresponding orbital transformation (COT) which, from the corresponding orbital overlaps, displays whether the system should be described as a spin-coupled or a closed-shell solution.

Results and Discussion

(a) Synthesis. The ligand 4,6-di-*tert*-butyl-2-[(pentafluorophenyl)amino]benzenethiol, H_2L, has been synthesized according to Scheme 3. It is a yellow powder which was stored under an Ar atmosphere.

From the reaction of 2 equiv of H_2L and 1 equiv of anhydrous $FeBr_2$ in acetonitrile in the presence of 4 equiv of triethylamine under anaerobic conditions, a brown solution was obtained which turned into deep purple upon brief exposure to air. The addition of $[PPh_4]Br$ produced a purple powder of $[PPh_4][FeL_2]$ (**1**). Complex **1** dissolved in CH_2Cl_2 can be readily oxidized with iodine to the neutral species $[FeI(L^{\bullet})_2]_0$ (**2**) which was isolated as black microcrystalline powder.

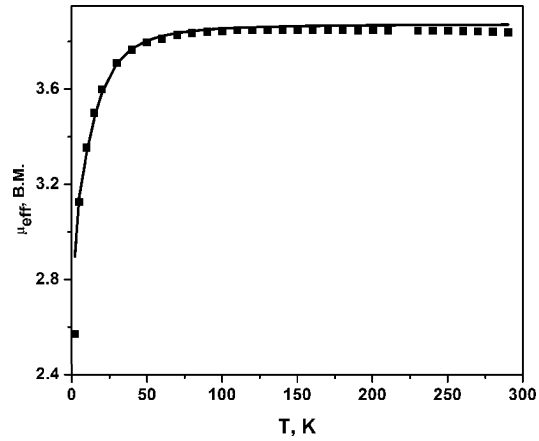

Figure 1. Temperature-dependence of the effective magnetic moment, μ_{eff}, BM, of a solid sample of **1**. Filled squares represent experimental data; the solid line is a best fit with $S = {}^3/_2$, $g = 2.00$ (fixed), $D = 18.0$ cm^{-1}, and $E/D = 0.19$ (E/D and the sign of D are derived from EPR).

$$\mathbf{1} + I_2 \rightarrow [Fe^{III}I(L^{\bullet})_2]^0 + [PPh_4]^+ + I^- \qquad (1)$$

This oxidation of **1** to **2** is entirely ligand-based as is shown below. The closed-shell ligand dianions in **1** are oxidized to the corresponding π radical monoanions $(L^{\bullet})^{1-}$, whereas the central metal ion in both **1** and **2** possesses a +III oxidation state. Similar complexes have been described recently.[8,21,22]

The cyclic voltammogram of **1** in CH_2Cl_2 solution (0.10 M $[N(n\text{-}Bu)_4]PF_6$) at 20 °C and a scan rate of 100 mV s^{-1} displays a reversible one-electron wave at −0.40 V vs Fc^+/Fc which corresponds to the couple $[\mathbf{1}]^0/[\mathbf{1}]^{1-}$ (see Supporting Information). An irreversible reduction peak is observed at −1.56 V vs Fc^+/Fc (see Supporting Information). For the neutral complex, we propose the following electronic structure: $[Fe^{III}(L)(L^{\bullet})]^0$ with a central intermediate spin ferric ion ($S_{Fe} = {}^3/_2$) coupled antiferromagnetically to a π radical ligand anion ($S_{rad} = {}^1/_2$) yielding an $S_t = 1$ ground state.

Finally, the reaction of 2 equiv of H_2L with 1 equiv of $PtCl_2$ in dry acetonitrile in the presence of 2 equiv of NEt_3 yields a brown solution from which upon exposure to air the dark green, diamagnetic microcrystalline $[Pt(L^{\bullet})_2]$ (**3**) was obtained. Similar complexes have also been reported previously.[23]

(b) EPR Spectroscopic Characterization and Magnetism of 1 and 2. Figure 1 shows the temperature-dependence of the effective magnetic moments of **1** in the range of 2−300 K in a 1.0 T external field. A fit of the data of **1** clearly establishes an $S_{Fe} = {}^3/_2$ intermediate spin ground state ($g = 2.0$; $|D| = 18.0$ cm^{-1}; $E/D = 0.19$). Complex **2** possesses an

(18) (a) Eichkorn, K.; Weigend, T.; Treutler, O.; Ahlrichs, R. *Theor. Chem. Acc.* **1997**, *97*, 119. (b) Eichkorn, K.; Treutler, O.; Ohm, H.; Haser, M.; Ahlrichs, R. *Chem. Phys. Lett.* **1995**, *242*, 652. (c) Eichkorn, K.; Treutler, O.; Ohm, H.; Haser, M.; Ahlrichs, R. *Chem. Phys. Lett.* **1995**, *240*, 283.

(19) Sinnecker, S.; Slep, L. D.; Bill, E.; Neese, F. *Inorg. Chem.* **2005**, *44*, 2245.

(20) (a) Noodleman, L.; Peng, C. Y.; Case, D. A.; Movesca, J. M. *Coord. Chem. Rev.* **1995**, *144*, 199. (b) Noodleman, L.; Case, D. A.; Aizman, A. *J. Am. Chem. Soc.* **1988**, *110*, 1001. (c) Noodleman, L.; Davison, E. R. *Chem. Phys.* **1986**, *109*, 131. (d) Noodleman, L.; Norman, J. G.; Osborne, J. H.; Aizman, A.; Case, D. A. *J. Am. Chem. Soc.* **1985**, *107*, 3418; Noodleman, L. J. *Chem. Phys.* **1981**, *74*, 5737.

(21) (a) Chun, H.; Bill, E.; Weyhermüller, T.; Wieghardt, K. *Inorg. Chem.* **2003**, *42*, 5612. (b) Chun, H.; Weyhermüller, T.; Bill, E.; Wieghardt, K. *Angew. Chem., Int. Ed.* **2001**, *40*, 2489.

(22) Chlopek, K.; Bill, E.; Weyhermüller, T.; Wieghardt, K. *Inorg. Chem.* **2005**, *44*, 7087.

(23) Herebian, D.; Bothe, E.; Bill, E.; Weyhermüller, T.; Wieghardt, K. *J. Am. Chem. Soc.* **2001**, *123*, 10012.

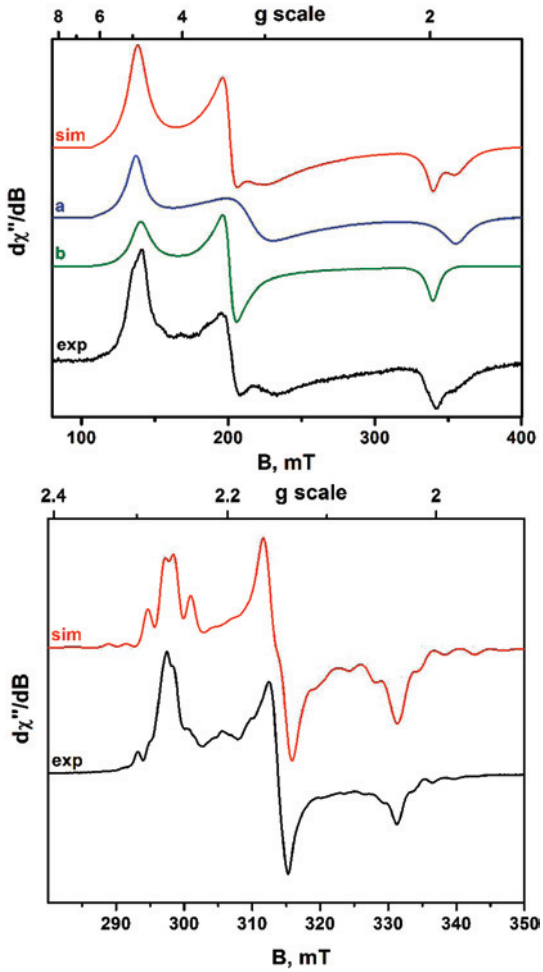

Figure 2. Top: Experimental X-band EPR spectrum of **1** in CH_2Cl_2 at 10 K. Experimental (black) conditions: frequency 9.45507 GHz; power 0.20 mW; modulation 1.5 mT. The simulation (red) is a 60/40 superposition of two subspectra assigned to the isomers **a** (in blue) and **b** (in green) with parameters given in the text. Bottom: X-band EPR spectrum of a frozen CH_2Cl_2 solution of **2** at 10 K. Experimental conditions: frequency 9.4348 GHz; power 0.20 mW; modulation 1.0 mT. Red: simulation (see text). Black: experimental spectrum.

$S_t = {}^1/_2$ ground state (data not shown), and complex **3** is diamagnetic ($S = 0$) as was judged from its "normal" ^{1}H NMR spectrum (see Experimental Section). The spin states of $S = {}^3/_2$ for **1** and $S = {}^1/_2$ for **2** have been confirmed by their X-band EPR spectra recorded in frozen CH_2Cl_2 solution; they are shown in Figure 2.

The experimental spectrum of a frozen CH_2Cl_2 solution of **1** at 10 K reveals a rhombic absorption pattern with effective g values around $g' = 4$ and 2. The values are typical of resonances within the $m_s = \pm{}^1/_2$ Kramers doublet of $S = {}^3/_2$ with large zero-field splitting and moderately strong rhombicity E/D. Because the spectrum is detected at liquid helium temperature, $m_s = \pm{}^1/_2$ must be the ground doublet, according to a positive D value. However, the appearance of line splittings, particularly at $g' = 2$ reveals the presence of two isomers in the sample with slightly different properties. This is corroborated by a simulation with two subspectra, **a** and **b**, with relative intensities of 60% and 40%, respectively. The effective g values for **a** are found at: $g'_x = 3.14$, $g'_y = 4.90$, $g'_z = 1.90$, and for **b**: $g'_x = 3.36$, $g'_y = 4.82$, $g'_z = 1.99$. Interestingly, the EPR spectrum of the analogous planar complex $[Fe^{III}L]^{1-}$ containing a tetraanionic porphyrinogen macrocycle $(L)^{4-}$ is axial with observed g values of 4.2 and 1.95 in accordance with its molecular D_{2d} symmetry.[2] In contrast, the cis-configured anion in **1** (Formula 1) is of lower symmetry (C_{2h}), and therefore, the EPR signal is rhombic. In solution this anion exists in two geometrical isomers, a trans-configured geometrical isomer (C_{2h}) and a cis-configured one (C_{2v}), both of which would give rise to a rhombic signal with similar g-values (as is observed). We cannot assign subspectra **a** or **b** to the trans or cis isomer at this point.

Formula 1

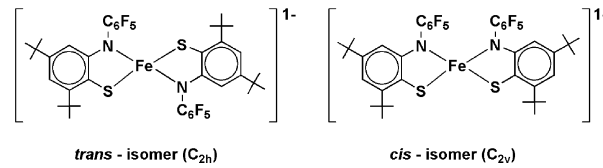

As we have shown previously for a series of five-coordinate, neutral $[Fe^{III}I(L^{\bullet})_2]$ complexes[8,21−23] with a doublet ground state ($S = {}^1/_2$), the EPR spectra provide direct spectroscopic evidence for the presence of two ligand π radicals, $(L^{\bullet})^{1-}$ ($S_{rad} = {}^1/_2$), and a central, intermediate spin ferric ion ($S_{Fe} = {}^3/_2$). The structure of the resulting total ground state, namely, $S = {}^1/_2$, is characterized by an antiferromagnetic alignment of the type [↓($S_{Rad} = {}^1/_2$), ↑($S_{Fe} = {}^3/_2$), ↓($S_{Rad} = {}^1/_2$)] which is caused by a strong antiferromagnetic iron−ligand radical exchange interaction dominating the inferior π radical−π radical interaction.

The spectrum of **2** displays a well resolved hyperfine splitting pattern of ∼8−9 lines at g_{min} and g_{max} (Figure 2 bottom). This hyperfine splitting cannot be due to hyperfine interactions to ^{14}N or ^{1}H nuclei because the central line at g_{min} is not split. Instead, we observe a strong hyperfine interaction with the apical ^{127}I ($I = {}^5/_2$, 100% natural abundance), which is affected by electric quadrupole interactions. A satisfactory fit was obtained by using the following parameters: (1) $g_{max} = 2.263$, $g_{mid} = 2.147$, $g_{min} = 2.034$, (2) A-tensor components along the principal g values according to $A = (19, -28, 7) \times 10^{-4}$ cm^{-1}, and (3) the traceless quadrupole coupling matrix, $P = (13, 10, -23) \times 10^{-4}$ cm^{-1}. (The sign of the main component of P is arbitrary, but it is significant that the major and minor components of g-matrix, A-tensor and P-tensor do not coincide.) Similar fits have been reported for the EPR spectra of complexes containing o-iminobenzosemiquinonato(1−),[21] o-iminothiobenzosemiquinonato(1−)[8] or o-diiminobenzosemiquinonato(1−) π radicals,[22] and an intermediate spin ferric ion $[Fe^{III}I(L^{\bullet})_2]^0$.

(c) Electronic Spectra of 1, 2, and 3. Figure 3 exhibits the electronic spectra of **1** and **2** in the range of 300−1100 nm. The spectrum of **1** displays transitions in the visible at 539 nm ($\varepsilon = 3.5 \times 10^3$ M^{-1} cm^{-1}) and a shoulder at ∼620 nm ($\varepsilon = 2.3 \times 10^3$ M^{-1} cm^{-1}), which we assign as ligand-to-metal charge transfer (LMCT) bands. This assignment has been confirmed by time-dependent density functional theo-

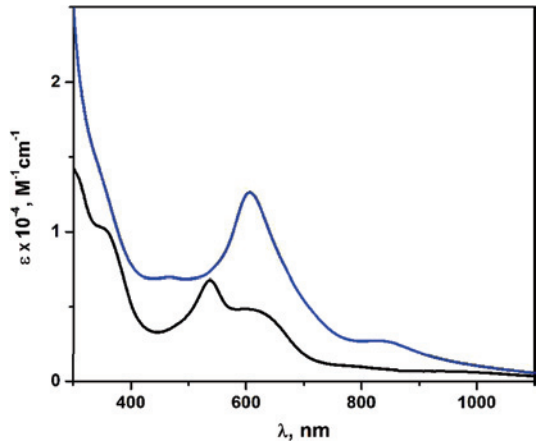

Figure 3. Electronic spectra of **1** (black) and **2** (blue) in CH_2Cl_2 solutions at 20 °C.

Table 2. Experimental and Calculated Zero-Field Mössbauer Parameters for Four- and Five-Coordinate Iron Complexes

	δ, mm s^{-1} [a]		ΔE_Q, mm s^{-1} [b]		
complex	exptl	calcd	exptl	calcd	S_t [c]
1	0.23	0.26	4.55	3.70	$^3/_2$
2 [d]	0.19	0.19	2.68	2.44	$^1/_2$
$[Fe^{III}(TipssiPP)]^+$	0.33[e]		5.16[e]		$^3/_2$
A	0.37	0.30	3.02	4.40	$^3/_2$
B	0.35		3.31		0
C[f]	0.30		2.71		0
D[g]	0.34		2.94		$^3/_2$

[a] Experimental isomer shift at 80 K vs α-Fe at 298 K. [b] Quadrupole splitting. [c] Ground state. [d] This complex is probably square pyramidal (five-coordinate). [e] Recorded at 6 K, ref 3. [f] Ref 8b. [g] Ref 9.

Table 3. Selected Bond Distances (Å) for **1** and **3**

complex **1**			
Fe1−N8	1.896(2)	S1−C2	1.774(2)
Fe1−S1	2.2044(5)	C2−C3	1.411(2)
C2−C7	1.414(2)	C3−C4	1.402(2)
C4−C5	1.397(3)	C5−C6	1.392(3)
C6−C7	1.399(3)	C7−N8	1.407(3)
N8−C9	1.411(3)		
complex **3**			
Pt1−N8	1.971(2)	S1−C2	1.719(3)
Pt1−S1	2.2520(7)	C2−C7	1.425(4)
C2−C3	1.426(4)	C3−C4	1.379(4)
C4−C5	1.413(4)	C5−C6	1.370(4)
C6−C7	1.408(4)	C7−N8	1.370(3)
N8−C9	1.420(3)		

retical calculations.[24] The strong absorption band in the spectrum of **2** at 604 nm ($\varepsilon = 1.3 \times 10^4$ M^{-1} cm^{-1}) may be assigned to a ligand-to-ligand charge transfer (LLCT). This band has also been observed in the spectrum of **3** at 841 nm ($\varepsilon = 8.1 \times 10^4$ L mol^{-1} cm^{-1}).[23]

(d) Mössbauer Spectra. Mössbauer parameters of complexes are given in Table 2. The zero-field Mössbauer spectrum of **1** displays a quadrupole doublet at 80 K with an isomer shift $\delta = 0.23$ mm s^{-1} and a large quadrupole splitting parameter $|\Delta E_Q| = 4.55$ mm s^{-1}. Similarly, the Mössbauer spectrum of **2** at 80 K displays a single quadrupole doublet with $\delta = 0.19$ mm s^{-1} and $|\Delta E_Q| = 2.68$ mm s^{-1}. It is remarkable that the isomer shift of **1** and **2** are quite

(24) We thank Dr. Vinzenz Bachler for the calculations (unpublished results).

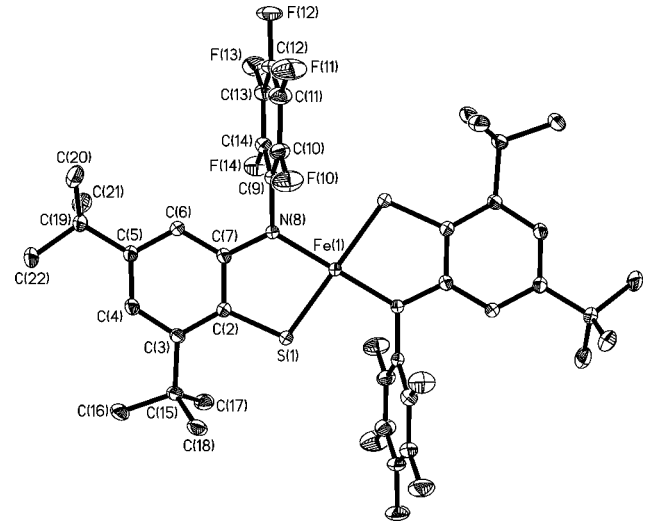

Figure 4. Perspective view of the monoanion in crystals of **1**.

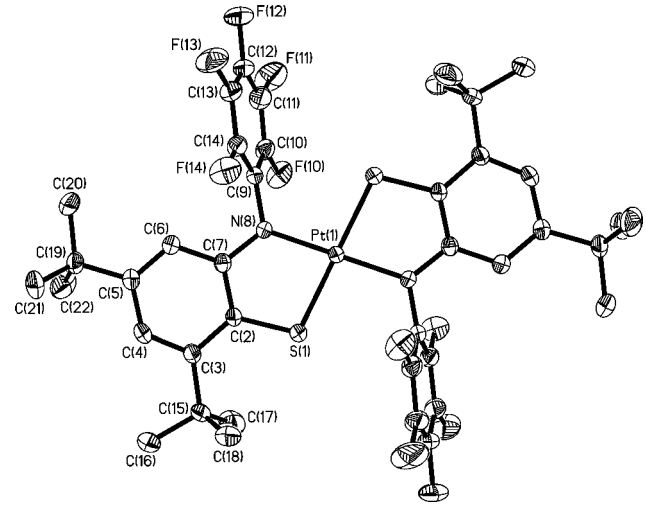

Figure 5. Perspective view of the neutral molecule in crystals of **3**.

similar; they support the notion that the intrinsic spin ground state of the respective iron ion in both complexes is the same, namely, intermediate spin ferric ($S_{Fe} = {}^3/_2$).[5] In **2**, the observed $S_t = {}^1/_2$ ground state is then attained via intramolecular antiferromagnetic coupling of two π radical ligand anions $(L^{\bullet})^{1-}$ to the ferric ion.[8,21,22]

(e) Crystal Structures. The crystal structures of **1** and **3** have been determined by single crystal X-ray crystallography at 100(2) and 190(2) K, respectively. Table 1 summarizes crystallographic details, and Table 3 gives selected bond distances. Figures 4 and 5 display the structures of the monoanion in **1** and of the neutral complex in **3**, respectively.

Crystals of $\mathbf{1}\cdot(C_2H_5)_2O$ consist of well separated tetraphenylphosphonium cations and $[Fe^{III}L_2]^{1-}$ monoanions and a solvent molecule of diethylether. The *trans*-FeS_2N_2 coordination geometry of the monoanion is square planar. There is no donor atom within bonding range of the iron ion (<4.0 Å) above and below the *trans*-FeS_2N_2 plane. There are two crystallographically independent monoanions in the unit cell of the triclinic space group $P\bar{1}$ (No. 2). Both iron ions are located on crystallographic inversion centers. It is interesting to note that the two planes of the *N*-pentafluorophenyl

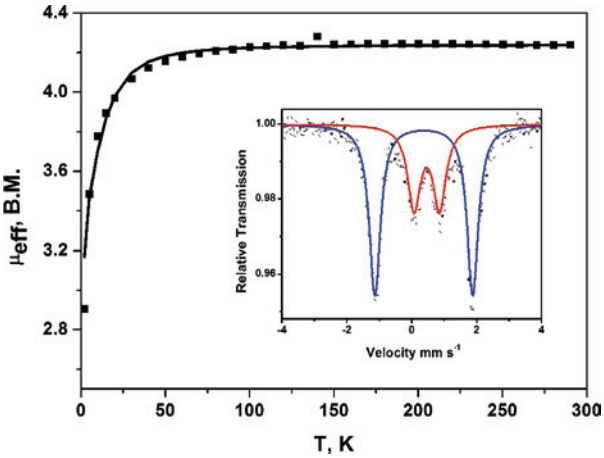

Figure 6. Temperature-dependence of the effective magnetic moment of a fresh sample of [N(*n*-Bu)$_4$][Fe^{III}(qdt)] (**A**): squares are experimental data; the red line represents a fit where a value for $\chi_{TIP} = 1140 \times 10^{-6}$ cm^3 mol^{-1} has been subtracted, $g = 2.19$. A zero-field splitting parameter $|D| = 16.2$ cm^{-1} has been established. Inset: Zero-field Mössbauer spectrum of the same sample at 80 K. Two subspectra are observed (a) $\delta = 0.37$ mm s^{-1}, $\Delta E_Q = 3.02$ mm s^{-1} (65%); (b) $\delta = 0.46$ mm s^{-1}, $\Delta E_Q = 0.78$ mm s^{-1} (35%); the latter corresponds to colloidal FeO(OH). The contribution of the contaminant was subtracted from the magnetic susceptibility data of the sample according to the molar ratio given by the Mössbauer spectrum and using the magnetic measurement of "rust" given in the Supporting Information.

substituents are nearly exactly perpendicular to the two planes of the five-membered chelate rings of the bis(*o*-aminobenzenethiolato)iron anion. Thus, these two bulky substituents are responsible for the stabilization of the *mononuclear* $[FeL_2]^{1-}$ arrangement because they effectively prevent the otherwise frequently observed dimerization.[1]

The neutral molecules in **3** are also square planar, with the intraligand bond distances clearly indicating the presence of two π radical monoanions $(L^{\bullet})^{1-}$. Most significantly, the two average C−S bond distances at 1.774(2) Å in **1** and 1.719(3) Å in **3** are different (outside 3σ limits) as are the C−N bond lengths at 1.407(2) Å in **1** and 1.370(3) Å in **3**. Furthermore, the six-membered aromatic rings in **3** exhibit distortions typical of quinoidal type structures, namely two shorter C═C and four longer ones.[8,22] This pattern is not present in **1**, which has no π radical ligands.

(f) Complexes from Ref 1 Revisited. The two complexes **A** and **B** from ref 1 have been prepared with slight modifications to the published recipe. The procedure for the monomer **A**, however, proved to be rather complicated and not quite reproducible. Apparent decomposition of complexes in solution due to the addition of aqueous NH_3 leads to the formation of significant and varying amounts of a high spin ferric impurity. For example, the Mössbauer spectrum of a freshly prepared, black microcrystalline is shown in the inset of Figure 6. It displays two quadrupole doublets: the first constitutes 65% iron of the sample with $\delta = 0.37$ mm s^{-1} and $|\Delta E_Q| = 3.02$ mm s^{-1} and the second (∼35%) with $\delta = 0.46$ mm s^{-1} and $|\Delta E_Q| = 0.78$ mm s^{-1} at 80 K. The latter is the same impurity found in the spectrum of the dimer **B** (Supporting Information, Figure S4) and is also present in the spectrum of **1** (Supporting Information, Figure S3). The ratio of the two signals of freshly prepared samples varies considerably. Theorizing that this impurity is colloidal iron oxide hydroxide (rust) particles, commonplace for iron chemistry conducted in basic media, the reaction was repeated sans the addition of ligand. Anhydrous $FeCl_3$ was dissolved in MeOH and treated with several drops of aqueous ammonia. Over the period of 1 h the solution became turbid as an orange precipitate evolved. Its Mössbauer spectrum afforded a single quadrupole doublet with an isomer shift $\delta = 0.48$ mm s^{-1} and a quadrupole splitting $|\Delta E_Q| = 0.65$ mm s^{-1} at 80 K (Supporting Information, Figure S7). A colloidal sample in MeOH gave very similar values ($\delta = 0.48$ mm s^{-1}, $|\Delta E_Q| = 0.72$ mm s^{-1} (Supporting Information, Figure S8)) that exactly match the high spin impurity found in the Mössbauer spectra of freshly prepared **A**, recrystallized **A,** and **B**. The magnetic susceptibility of the precipitate is rather low, according to the presumed oxide structure for which antiferromagnetic exchange coupling of adjacent ions quenches most of the spin moments. On the basis of the adopted molar mass of 88.6 g mol^{-1} for FeO(OH), we found an effective magnetic moment of 1−1.2 μ_B per iron in the range 100−300 K, and a gradual drop below 50 K (see Supporting Information, Figure S9). The high temperature values corresponds to about 0.4 spins ($S = {}^1/_2$) per ferric ion. Therefore the contribution of the corresponding rust contaminant to the magnetic susceptibility data of **A**, **B**, and **1** is very small.

Figure 6 shows the temperature-dependence of the magnetic moment of the freshly prepared sample from above. The minute contribution of colloidal impurity of FeO(OH) to the sample magnetization has been subtracted from the measurement. The resultant temperature-independent magnetic moment of ∼4.2 μ_B between 50 and 290 K immediately rules out the presence of the dimer [N(*n*-Bu)$_4$]$_2$[Fe$^{III}_2$(qdt)$_4$] (Supporting Information, Figure S6). It is characteristic for an intermediate spin ferric ion as in **1**. Below 50 K, a zero-field splitting of $|D|_{3/2} = 16.2$ cm^{-1} ($g = 2.19$) has been established. Thus, the monomeric monoanion [Fe^{III}(qdt)$_2$]$^{1-}$ possesses an $S_{Fe} = {}^3/_2$ ground state as has been found for **1**, where a similar zero-field splitting parameter was determined. Recrystallization of **A**, containing the structurally characterized monomeric monoanion [Fe^{III}(qdt)$_2$]$^{1-}$ from a CH_3OH/water mixture with trace amounts of aqueous ammonia, significantly decreased the amount of rust in the sample (<10%) (Supporting Information, Figure S5).

The dimeric complex **B** has been obtained from a solution of quinoxalinedithiol in dry CH_3OH to which 2 equiv of $NaOCH_3$ had been added. A solution of $FeCl_3$ in dry CH_3OH was then added dropwise over a period of 10 min. After filtration, a solution of [PPh$_4$]Br (1 equiv) was added to the filtrate, and water was added dropwise to afford the precipitation of the salt [PPh$_4$]$_2$[Fe$^{III}_2$(qdt)$_4$] (**B**). Its zero-field Mössbauer spectrum exhibits a single quadrupole doublet with an isomer shift $\delta = 0.35$ mm s^{-1} and a rather large quadrupole splitting $|\Delta E_Q| = 3.31$ mm s^{-1} at 80 K (Supporting Information, Figure S1). A 9% rust impurity was also observed ($\delta = 0.47$ mm s^{-1}, $|\Delta E_Q| = 0.73$ mm s^{-1}). The above Mössbauer parameters for the dimeric dianion in crystalline **B** are very similar to those reported for [NEt$_4$]$_2$[Fe$^{III}_2$(mnt)$_4$] (mnt^{2-} = maleonitriledithiolate(2−)):

$\delta = 0.33$ mm s^{-1}, $|\Delta E_Q| = 2.81$ mm s^{-1} at 77 K,[25] and the neutral complex **C** with $\delta = 0.30$ mm s^{-1}, $|\Delta E_Q| = 2.71$ mm s^{-1}.[8b] The five-coordinate monomeric species **D** also possesses an intermediate spin $S_{Fe} = {}^3/_2$ ground state and displays again very similar Mössbauer parameters: $\delta = 0.33$ mm s^{-1}, $|\Delta E_Q| = 3.02$ mm s^{-1}.[9]

Formula 2

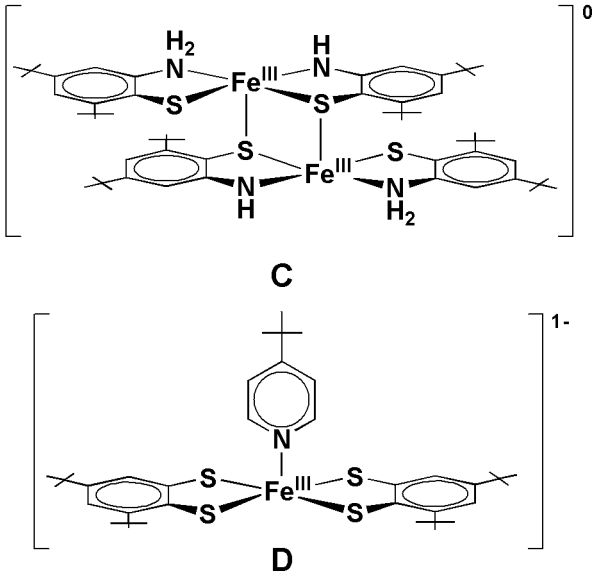

Therefore, we conclude that the central iron ions in **B**, **C**, and **D** possess the same intrinsic intermediate spin ground state ($S_{Fe} = {}^3/_2$). In the dimer **B**, it is expected that the two ferric ions in the dianion couple antiferromagnetically affording a diamagnetic ground state ($S_t = 0$).

Figure 7 exhibits the temperature-dependence of the magnetic moment of solid **B**. We have been able to model the experimental data for a dimeric species by using the exchange Hamiltonian $H_{ex} = -2JS_1 \cdot S_2$ ($S_1 = S_2 = {}^3/_2$), $g = 2.0$. The offset of μ_{eff} at $T < 50$ K, which indicates a paramagnetic impurity was assigned to a contribution from monomers **A** ($S = {}^3/_2$, ~5% per weight). From these data an antiferromagnetic coupling constant of $J = -94$ cm^{-1} has been established for **B**, which resembles closely values reported for similar dimeric species.[9]

Monomeric **A** and dimeric **B** exist in delicate equilibrium in solution. This can be inferred from the Mössbauer parameters of the recrystallized complex **A**, which are noticeably different to those of monomer **A**: now the parameters at $\delta = 0.34$ mm s^{-1} and $|\Delta E_Q| = 3.42$ mm s^{-1} at 80 K indicate the presence of the *dimer* in [N(*n*-Bu)$_4$]$_2$[Fe$^{III}_2$(qdt)$_4$] as in **B** (Supporting Information, Figure S4). This is further corroborated by the X-band EPR measurements in THF and MeOH at 10 K. Both recrystallized **A** and dimeric **B** produced no EPR signal in THF, as is expected for diamagnetic compounds. However, in MeOH,

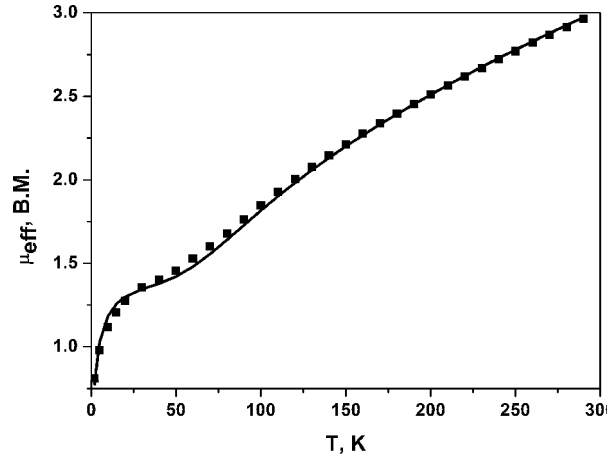

Figure 7. Temperature-dependence of the effective magnetic moment of **B** (squares represent experimental data). The solid line represents a best fit to the Hamiltonian $H_{ex} = -2JS_1 \cdot S_2 + g\mu_B(S_1 + S_2)B$ with $S_1 = S_2 = {}^3/_2$, $g = 2.0$, $J = -94$ cm^{-1}. The experimental data are corrected for diamagnetic contributions and temperature-independent paramagnetism ($\chi_{TIP} = 291 \times 10^{-6}$ cm^{-3} mol^{-1}). A 10% paramagnetic impurity with $S = {}^3/_2$ was added to the simulation, for which a Weiss constant (θ) of -5 K has been adopted. (The contribution of the 9% ferric (oxide) contaminant found in the Mössbauer spectrum (Supporting Information, Figure S4) was neglected in the analysis of the magnetic data, because the contribution to the sample mass was only 0.6%, based on the molar mass of FeO(OH) (88.6 g mol^{-1} with 0.4 spins ($S = {}^1/_2$) per iron; see Supporting Information).

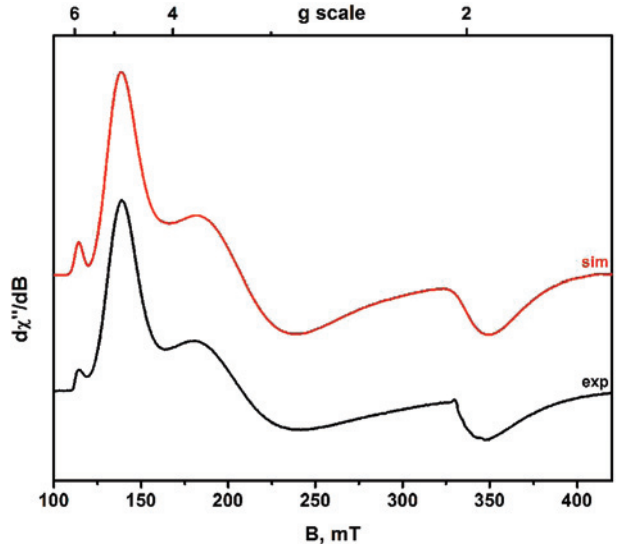

Figure 8. X-band EPR spectrum of **A** in MeOH at 10 K (Experimental conditions: frequency 9.4306 GHz; power 0.63 mW; modulation 0.2 mT). The red line is a spin Hamiltonian simulation for $S = {}^3/_2$ with $D = 2$ cm^{-1}, $E/D = 0.148$, $g = (2.042, 2.042, 2.019)$. A Gaussian distribution of the rhombicity parameter has been invoked to account for the line shape of frozen solution with half-width $\sigma(E/D) = 0.052$. Note the intensity of the resolved peak at $g' = 6$ from the excited $m_s = \pm{}^3/_2$ Kramers doublet is an excellent marker for the size of the zero-field splitting.

an $S = {}^3/_2$ signal was observed with characteristic effective g values: $gx' = 3.28$, $gy' = 4.87$, $gz' = 1.94$. These parameters are somewhat different to those describing **A**, most notably when the spectrum is simulated with $S = {}^3/_2$, as shown in Figure 8. The obtained zero-field splitting parameter $D = +2.0$ cm^{-1} is much smaller compared to the magnetic susceptibility measurements of **A** (vide supra). In MeOH, the dimer is cleaved and forms an intermediate spin ferric species with a weakly coordinated methanol ligand. The difference in D clearly discriminates the species from

(25) (a) Koch, S. A.; Maelia, L. E.; Millar, M. *J. Am. Chem. Soc.* **1983**, *105*, 5944. (b) Deaton, J. C.; Gebhard, M. S.; Koch, S. A.; Millar, M.; Solomon, E. I. *J. Am. Chem. Soc.* **1988**, *110*, 6241. (c) Gebhard, M. S.; Deaton, J. C.; Koch, S. A.; Millar, M.; Solomon, E. I. *J. Am. Chem. Soc.* **1990**, *112*, 2217.

Table 4. Experimental (80 K) and Calculated Mössbauer Parameters

	experimental		calculated		
complex	δ, mm s^{-1}	ΔE_Q, mm s^{-1}	S_{Fe}	δ, mm s^{-1}	ΔE_Q, mm s^{-1}
1	0.23	4.55	$^1/_2$	0.31	−0.72
			$^3/_2$	**0.26**	**3.70**
			$^5/_2$	0.26	−1.73
2	0.19	2.68	**$^1/_2$**	0.19	2.44
A	0.37	3.02	$^1/_2$	0.33	1.41
			$^3/_2$	**0.30**	**4.40**
			$^5/_2$	0.25	−1.50
B	0.35	3.31	**$^3/_2$**	0.29	3.32

the alternative quasi planar iron complexes, for which the ligand-field splitting also induces $S = {}^3/_2$ because of the "1 over 4" orbital splitting pattern. In the quasi planar coordination without π-interaction to axial ligands the zero-field splitting is much larger, apparently due to reduced splitting of the four populated d orbitals, which enables much stronger effects of spin–orbit coupling.

(g) DFT Calculations. The ground state geometries of complex **1** and its dithiolato analogue **A** have been optimized assuming (a) the presence of a central, intermediate spin iron(III) $S = {}^3/_2$ by using the spin-unrestricted Kohn−Sham density functional B3LYP, (b) a broken symmetry BS(4,1) $M_S = {}^3/_2$ model for a high spin ferrous ion ($S_{Fe} = 2$) and an antiferromagnetically coupled ligand π radical ($S_{rad} = {}^1/_2$), (c) a BS(2,1), $M_S = {}^1/_2$ model with an intermediate spin ferrous ion ($S_{Fe} = 1$) and a ligand π radical yielding an $S_t = {}^1/_2$ ground state, (d) a spin-unrestricted $S = {}^1/_2$ model, and (e) a high spin ferric $S = {}^5/_2$ model. The most salient result is that both **1** and [Fe^{III}(qdt)$_2$]$^{1-}$ possess an intermediate spin ground state. This $S = {}^3/_2$ model is lower in energy by ~6 kcal mol^{-1} for both **1** and **A** than the corresponding high spin model ($S = {}^5/_2$). Most significantly, the low-spin ferric model ($S = {}^1/_2$) is 8.5 kcal mol^{-1} higher in energy for **1** and 16.6 kcal mol^{-1} for **A** than the $S = {}^3/_2$ model. These calculated results correlate with the spectroscopic data such that we can conclude that *for square planar* **1** and **A** the intermediate spin $S = {}^3/_2$ *ferric model represents the ground state.*

As shown in the Supporting Information, the agreement of structural parameters (bond lengths), between experiment and calculations for both anions **1** and **A** is excellent. The C−C, C−S, and C−N bond distances agree within ±0.01 Å, whereas the calculated Fe−S and Fe−N bond distances are overestimated by maximally 0.08 Å, which is a typical result for the B3LYP functional.

To calibrate the above electronic structures we have also calculated the Mössbauer parameters of the two complexes (**1** and **A**) for both an $S = {}^3/_2$ intermediate spin ferric model and for an $S = {}^1/_2$ ground state (Table 4), and for **1**, this gives excellent agreement with experiment. Likewise, for **A**, the results for the $S = {}^3/_2$ model are in reasonable agreement with the experimental data. A distinctly different quadrupole splitting is calculated for an $S = {}^1/_2$ ground state.

Figure 9 shows the Mulliken spin density plots for the anions in **1** and **A**, respectively. In both cases three unpaired electrons are localized at the ferric ion and the qualitative bonding schemes derived from the spin-unrestricted S = $^3/_2$ calculations of **1** and **A** (Supporting Information) show each

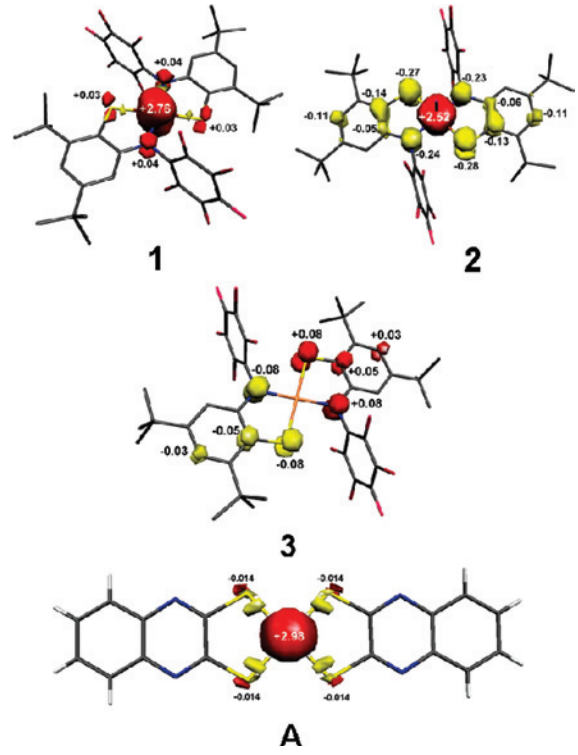

Figure 9. Spin density plots from Mulliken spin population analyses of **1**, **2**, **3**, and **A** (red α-spin; yellow β-spin).

five metal-centered orbitals: three of these are half-filled SOMOs; one metal-d orbital (d_{xy}) is doubly occupied, and one metal-d orbital is empty. This is the hallmark of intermediate spin ferric ions in both species. Interestingly, the ligands in both **1** and **A** do not carry significant spin density; they are closed-shell dianions.

In contrast, the geometry optimization for **2** ($S = {}^1/_2$) using the BS(3,2) approach and the B3LYP functional and the standard spin-unrestricted $S = {}^1/_2$ model afforded the same energy minimum. Since there is no X-ray structure of **2** available, we cannot compare the calculated metrical details of the two organic ligands with experiment. Nonetheless, it is notable that the C−C, C−N, and C−S bond distances calculated for **2** agree very well with those found experimentally in **3** where two monoanionic ligand π radicals are present. The calculated electronic structure of **2** reveals a qualitative MO bonding scheme as shown in Figure 10.

Again five orbitals of predominantly metal-d character have been identified: one of them is found in the spin-up and spin-down manifold (doubly occupied MO), three Fe-based orbitals occur only the spin-up manifold (singly occupied MO's) and one metal-d orbital is empty. Thus, we identify an intermediate spin ferric ion. In addition, two singly occupied ligand MO's are identified in the spin-down manifold which are antiferromagnetically coupled to two metal-d SOMO's yielding the observed $S = {}^1/_2$ ground state of **2**. The Mulliken spin density plot is shown in Figure 9; complex **2** features an intermediate spin ferric ion coupled antiferromagnetically to two ligand π radicals (L$^{\bullet}$)$^{1-}$ as shown in ref 5 for similar complexes with *o*-aminothiophenolate(1−) radicals.

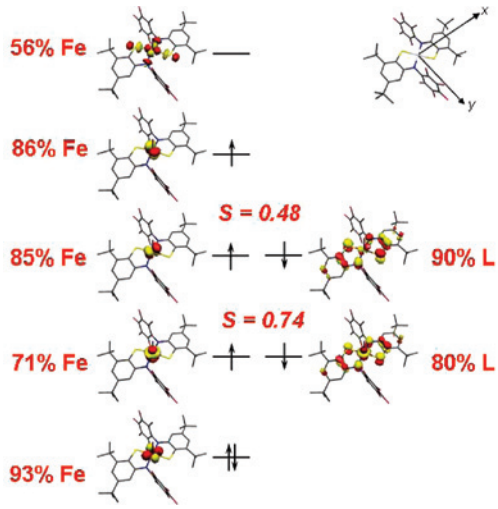

Figure 10. Qualitative MO scheme for neutral **2** ($S = {}^1/_2$) as derived from a BS(3,2) DFT calculation (B3LYP/ZORA).

Scheme 4. Selected Resonance Structures of π Radical Anion $(L^{\bullet})^{1-}$

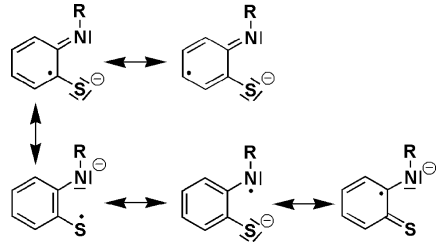

The ground state geometry of planar **3** has been optimized for a standard spin-unrestricted closed-shell model ($S = 0$) and a BS(1,1) $M_S = 0$ model for a singlet diradical (Supporting Information). The latter solution is found to be lower in energy by 14 kcal mol^{-1}. The agreement between experiment and calculation is excellent and allows a clear distinction between the closed-shell dianionic form of the ligand in **1** and its one-electron oxidized π radical in **2** and **3**. As shown in Scheme 4, these calculations for the π radical anion can be represented by the Lewis structures depicted below.

Figure 9 shows a spin density plot (Mulliken analysis) with α-spin density in red and β-spin density in yellow for **3**.

Conclusions

We have unambiguously shown that square planar ferric complexes with a d^5 electron configuration and a *trans*-$Fe^{III}N_2S_2$ geometry as in **1** and an $Fe^{III}S_4$ geometry as in **A** possess a central, intermediate spin ferric ion ($S_{Fe} = {}^3/_2$). We have not found evidence for the presence of a low spin configuration ($S = {}^1/_2$) for **A**. The dimeric dianion in **B** also contains intermediate spin ferric ions in a square pyramidal FeS_5 geometry as was judged by its Mössbauer parameters, which resemble closely those of **A**. It is interesting to note that all ferric complexes containing four monodentate benzenethiolate(1−)[25] or two *o*-xylyl-α,α′-dithiolate(2−)[26] ligands, namely, $[Fe^{III}(SR)_4]^{1-}$ or $[Fe^{III}(S_2\text{-}o\text{-xyl})_2]^{1-}$ species, possess a high spin configuration ($S_{Fe} = {}^5/_2$) and a *tetrahedral* FeS_4 polyhedron. The observed Mössbauer parameters $\delta = 0.13$ mm s^{-1} and $|\Delta E_Q| = 0.57$ mm s^{-1} at 77 K[26] are consistent with high spin ferric species with Fe(III)−S_4 units distorted from T_d symmetry.

Note that in these tetrahedral $Fe^{III}S_4$ species a single quadrupole doublet is observed with a *small* quadrupole splitting. In contrast, in square planar **A** the ferric ion possesses an intermediate spin ground state $S = {}^3/_2$ with Mössbauer parameters $\delta = 0.37$ mm s^{-1} and $|\Delta E_Q| = 3.02$ mm s^{-1}. Thus, a very large quadrupole splitting is observed.

In agreement with this, the average Fe−S distance in high spin, tetrahedral $[Fe^{III}(S_2\text{-}o\text{-xyl})_2]^{1-}$ is long at 2.268 Å[26] but somewhat shorter at 2.175 Å in intermediate spin, square planar **A**.[1] This is because the strongly antibonding $d_{x^2-y^2}$ metal orbital is half-occupied in the tetrahedral, high spin FeS_4 species but empty in the intermediate spin, square planar complex **A**.

Acknowledgment. N.R. and S.S. thank the Max-Planck-Society for a doctoral stipend and a postdoctoral fellowship, respectively. We are grateful for financial support from the Fonds der Chemischen Industrie.

Supporting Information Available: X-ray crystallographic files in CIF format for **1** and **3**, cyclic voltammograms of **3** and **1**, respectively, zero-field Mössbauer spectra of **1**, **2**, **B**, and **A**, the temperature-dependence of the magnetic moment of recrystallized **A**, zero-field Mössbauer spectra of solid and colloidal rust and its temperature-dependent magnetic moment, and tables of geometrical and electronic structural details of DFT calculations for **1**, **2**, **3**, and **A**. This material is available free of charge via the Internet at http://pubs.acs.org.

IC801109N

(26) (a) Lane, R. W.; Ibers, J. A.; Frankel, R. B.; Holm, R. H. *Proc. Nat. Acad. Sci. U.S.A.* **1975**, *72*, 2868. (b) Lane, R. W.; Ibers, J. A.; Frankel, R. B.; Papaefthymiou, G. C.; Holm, R. H. *J. Am. Chem. Soc.* **1977**, *99*, 84.